Available online at www.sciencedirect.com
ScienceDirect
Journal of Power Sources 174 (2007) 312–320
JOURNAL OF POWER SOURCES
www.elsevier.com/locate/jpowsour

Study of the Li^+ insertion into V_2O_5 films deposited by CVD onto various substrates

H. Groult [a,*], K. Le Van [a], A. Mantoux [b], L. Perrigaud [a], P. Doppelt [c]

[a] *Université P. & M. Curie-Paris6, CNRS-UPMC UMR 7612, Laboratoire LI2C, 4 Place Jussieu, Paris F-75005, France*
[b] *Science et Ingénierie des Matériaux et Procédés, INPGrenoble-CNRS-UJF, BP 75, 38402 Saint Martin D'Hères, France*
[c] *Centre d'Etude de Chimie Métallurgique, CNRS, 15 Rue G. Urbain, F-94407 Vitry sur Seine, France*

Received 14 May 2007; received in revised form 11 September 2007; accepted 16 September 2007
Available online 21 September 2007

Abstract

Vanadium oxide films were synthesised by chemical vapour deposition (CVD) from pure of triisopropoxyvanadium oxide ($VO(OC_3H_7)_3$) and oxygen as precursors. The influence of the substrate on the crystallinity of the vanadium oxide films was studied before and after annealing at 500 °C. On mica substrates, as-deposited film was composed of crystalline V_2O_5 as revealed by XRD. On Pt, Ti, stainless steel, glass and F-doped SnO_2 substrates, an annealing procedure was required to get V_2O_5. SEM investigations have clearly evidence V_2O_5 plates but the kinetics growth seems to be strongly dependent on the nature of the substrate. The insertion/extraction of Li^+ into the host structure was investigated in 1 M $LiClO_4$-PC with annealed V_2O_5 films deposited on Ti, Pt and stainless steel substrates. The best electrochemical performances were obtained in the potential range 3.8–2.8 V versus Li/Li^+ with V_2O_5 films deposited onto stainless steel substrate: the reversible capacity reaches after subsequent cycles was about 115 mAh g^{-1} (rate *C*/23). In a wider potential range (between 3.8 and 2.2 V versus Li/Li^+), V_2O_5 deposited onto Ti substrate exhibited the higher electrochemical performances (220 mAh g^{-1} for a rate of *C*/23).

Keywords: V_2O_5 films; Chemical vapour deposition; X-ray diffraction; Scanning electron microscopy; Lithium batteries

1. Introduction

The development of miniaturized electronic devices, notably in the field of microbatteries, have catalysed research programs all over the world to synthesis small energy sources with high power density. In that goal, many studies are devoted to the synthesis of thin films to be used as cathode materials in all solid-state batteries [1–4]. Several chemical and physical techniques can be employed for the synthesis of thin films such as sputtering, pulsed laser deposition, sol–gel, electron beam evaporation, atomic layer deposition and chemical vapour deposition with various successes. Concerning the choice of the electrode materials, transition metal oxides have been considered as the most suitable cathode materials in Li-ion batteries. Among these compounds, much attention has been paid to vanadium oxide (VOx) notably V_6O_{13} and amorphous or crystalline V_2O_5 [5–17] due to their high charge capacity, i.e. high capability to insert reversibly a high amount of lithium, the occurrence of potential plateau and good cycle life. For V_6O_{13} [12,13,15,18–22], the open circuit voltage (≈2.9 V versus Li/Li^+) is slightly lower than that observed with crystalline V_2O_5 (≈3.5 V versus Li/Li^+), but it exhibits higher theoretical reversible capacity of about 420 mAh g^{-1} which corresponds to a maximum of eight Li per mole of V_6O_{13} [15,19,20,23]. In the case of composite V_2O_5 electrode, the electroreduction of V_2O_5 can occur in a large potential window comprised between 3.5 and 1.5 V versus Li/Li^+ according to the following reaction:

$$V_2O_5 + y(Li^+ + e^-) \rightarrow Li_yV_2O_5 \quad (1)$$

where *y* is the insertion ratio of lithium per mole of V_2O_5. At the end of the discharge (1.5 V versus Li/Li^+), about three electrons per mole of V_2O_5 could be theoretically reached. However, the insertion of more than one lithium per mole of V_2O_5 induces usually irreversible structural changes which limit the working potential window for an extended use [24].

* Corresponding author. Tel.: +33 1 4427 3534; fax: +33 1 4427 3856.
E-mail address: groult@ccr.jussieu.fr (H. Groult).

0378-7753/$ – see front matter © 2007 Elsevier B.V. All rights reserved.
doi:10.1016/j.jpowsour.2007.09.045

The electrochemical performances of such VOx films versus Li^+ insertion/extraction are intimately related to their morphology and structure which are also strictly dependent on the deposition technique and the operating conditions. It is difficult to obtain directly crystalline VOx except in some cases [15,16] and as-deposited VOx films are usually amorphous. Therefore, an annealing procedure at high temperature in air is usually required to get crystalline V_2O_5. However, this treatment induces a high stress within the film, notably because of the difference of thermal expansion coefficient values for between the substrate and the VOx films. For example, it is reported that between 0 and 100 °C, the linear expansion coefficients are equal to $0.63 \times 10^{-6}\,C^{-1}$, $17 \times 10^{-6}\,C^{-1}$, $8.6 \times 10^{-6}\,C^{-1}$, $8.5 \times 10^{-6}\,C^{-1}$ and $9 \times 10^{-6}\,C^{-1}$ for V_2O_5, stainless steel, titanium, glass and Pt [25], respectively. This stress could drastically modify not only the structural properties and but also the adherence of the film onto the substrate during the Li^+ insertion/extraction. In other words, it could have a significant effect on the electrochemical performances of the cathode materials in Li-ion battery during cycle life. Thus, the dependence of choice of the substrate for the deposition of the VOx films used as positive electrode in lithium battery is a key parameter and must be considered very carefully. In that way, Julien et al. [17] have prepared VOx thin films by pulsed laser deposition (PLD) using various substrates and for different substrates temperature. They have shown that as-deposited films on silicon substrate maintained at room temperature are amorphous, as well as the films deposited onto glass substrate. In contrast, the films deposited onto silicon wafer heated at 300 °C evidence an orthorhombic polycrystalline phase. More recently, Kanno et al. [26] have studied the crystallinity of single-crystal thin films of layered $LiCoO_2$ and spinel $LiMn_2O_4$ onto a single crystal of $SrTiO_3$ by PLD and shown that the orientation of the deposited film is strictly controlled by the substrate plane.

As told before, among the different deposited materials, much attention has been paid to the study of vanadium oxides films due to their remarkable performances versus Li^+ insertion/extraction. But VOx can also be used for various important applications: as catalyst in oxidation reactions or for its electrochromism properties [27,28]. It is why the first part of this work has been devoted to a specific study of the influence of the nature of the substrate on the crystallinity of as-deposited and annealed vanadium oxide films synthesised by CVD. Then, the electrochemical properties (after annealing) of annealed VOx films deposited onto conducting substrates used as positive materials in lithium secondary batteries were studied. The main advantages of the CVD technique are the low operating deposition temperature, the low cost of the process, the possibility of controlling the chemical and physical properties of the films by a proper choice of the starting precursor and synthesis conditions [15]. Thus, it could give rise to various crystallinity and composition of the VOx films. The structural characterisations of VOx films were performed by X-ray diffraction and the morphological observations by scanning electron microscopy. Then, correlation between the physico-chemical characterisations and the electrochemical performances of annealed films versus the insertion/extraction of Li^+ in organic electrolyte were studied.

2. Experimental details

2.1. Films synthesis

An evaporator and a deposition device composed the deposition CVD system. A TriJet™ (or JIPELEC InJect) liquid delivery system has been used to supply and to vaporize the precursor solution into the reactor allowing a flash evaporation while keeping the rest of precursor stored under nitrogen in a glass container at room temperature [29].

The deposition of vanadium films were performed onto various substrates: Pt (sample A), Ti (sample B), stainless steel (sample C), F-doped SnO_2 (sample D), glass (sample E), mica (sample F) and Si (sample G). The electrochemical properties of the vanadium oxide films used as positive materials in Li-ion batteries were obviously investigated only on conducting foil substrates (Pt, stainless steel and Ti). Before deposition, the substrates were cleaned in hot dichloromethane, then in ethanol before rinsing with distilled water and finally dried under vacuum to remove traces of water.

The synthesis of VOx films has been achieved from reaction of vanadium(V) tri(isopropoxide)oxide (denoted $VO(OiPr)_3$ provided by Strem), and oxygen as reactant gas. The temperature of the precursor introduced into the evaporator was 84 ± 1 °C. Vapours were then dispatched until the deposition area by a constant flow of helium (10 sccm) used as carrier gas where they met oxygen. The flow rate of oxygen was 100 sccm and the total pressure in the CVD reactor was fixed to 18 Torr. The mixture of precursor and oxygen gas was introduced into the deposition chamber on the susceptor where the substrates heated at 300 °C were located. Finally, gaseous products resulting from deposition reaction reported above were trapped in liquid nitrogen present in a container situated in the outlet of the CVD reactor. The deposition time is only dependent on the injected pulses number and on the injection frequency.

A thermal annealing was performed at 500 °C in air during 2 h to obtain crystalline V_2O_5. To avoid shrinkage of the V_2O_5 film, the temperature was slowly raised to the desired temperature at a rate of $50\,°C\,h^{-1}$, i.e. the total annealing treatment times was 12 h. Then, a slow cooling procedure to room temperature was performed in order to obtain a good adhesion of the deposited films on the substrate.

For clarity, the annealed samples were denoted sample A500 for sample A heat-treated at 500 °C, sample B500 for sample B heat-treated at 500 °C, and so on, henceforth.

2.2. Physico-chemical characterisations

X-ray diffraction patterns were collected with a Siemens D5000 X-ray diffractometer ($\lambda_{K\alpha 1Co} = 1.7890$ Å) operating in the Bragg–Brentano type geometry. JCPDS data cards used for the indexing of the XRD peaks are 72-0433, 71-0454, 71-0424, 71-0040 and 85-1514 for V_2O_5, V_3O_7, V_4O_7, V_6O_{11} and V_5O_9, respectively. The crystallite sizes, L, of the V_2O_5 particles were calculated from the broadening of the corresponding ($h\,k\,l$) lines

according to Scherrer's formula:

$$L = \frac{0.89\lambda_1}{B\cos(\theta)} \quad (2)$$

where λ_1 is the wavelength of the $K_{\alpha 1Co}$ beam, θ the Bragg angle and B is the angular full width at half maximum (FWHM) intensity of the corresponding ($h\,k\,l$) diffraction line. Parameter B was corrected from the instrumental line broadening, b, according to the following equation [30]:

$$\beta = \sqrt{(B^2 - b^2)} \quad (3)$$

where b is 0.04°.

The uncertainty on all the reported XRD values was estimated to be 0.01 nm. The cell parameters were calculated using classical formula in considering that V_2O_5 crystallizes in orthorhombic.

A Jeol JEM 100 CX II transmission electron microscope equipped with a Jeol high resolution scanning attachment (STEM-SEM ASID 4D) was used for surface investigations by scanning electron microscopy.

2.3. Electrochemical tests

The electrochemical performances of crystalline V_2O_5 films versus the insertion/extraction of Li^+ were investigated in 1 M $LiClO_4$-PC solution (provided by Merck and used as received) by chronopotentiometry at room temperature in a glove box filled by argon ($C_{H_2O} \leq 5$ ppm) using Swagelock cells [31]. Both counter and reference electrodes were metallic lithium pellets. The galvanostatic charge–discharge curves and cyclic voltammograms were performed using a VMP Bio-Logic generator. Chronopotentiometry experiments were carried out at various constant current density between 3.8 and 2.8 V versus Li/Li^+ and 3.8–2.2 V versus Li/Li^+.

3. Results and discussion

3.1. SEM observations on annealed VOx films

SEM investigations were performed with annealed vanadium oxide films and we present here the images recorded with V_2O_5 films deposited onto Pt (sample A500), Ti (sample B500) and stainless steel substrate (sample C500) in Figs. 1–3, respectively. For each sample, low (bar scale: 2 μm) and high (bar scale: 200 nm) resolution images, as well as cross-section images were collected. These SEM images clearly showed the influence of the annealing on the morphology of the film depending on the substrate. Homogeneous and smooth V_2O_5 films surfaces were observed with Pt substrate (sample A500, Fig. 1a and b) and stainless steel substrate (sample C500; Fig. 3a and b). However, the images have pointed out the presence of many cracks on the surface for sample A500 (Fig. 1a), notably due to a highest difference of thermal expansion coefficients between V_2O_5 and Pt as reported above. In the case Ti substrate (sample B500), the roughness of the film (Fig. 2a and b) were drastically different from those observed with samples A500 and C500.

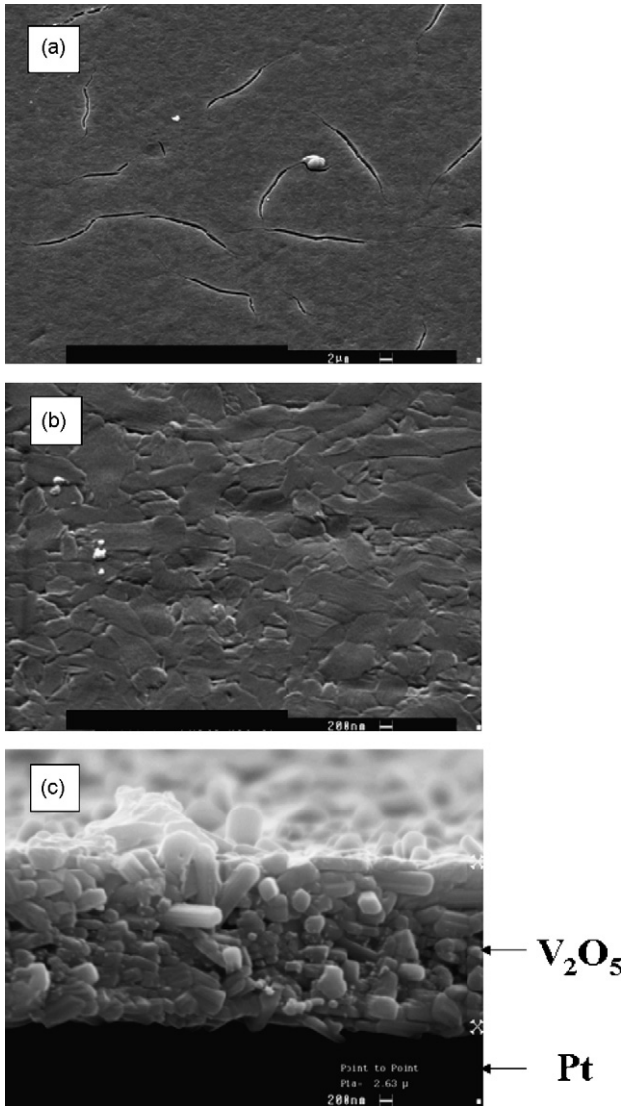

Fig. 1. SEM images of annealed V_2O_5 films deposited by CVD on platinum substrate (sample A500).

Whatever the substrate, the high resolution images (Figs. 1b, 2b, and 3b) revealed the presence of typical V_2O_5 plates [32]. The smallest particles size seems to be obtained for sample C500.

Cross-section images gave additional information concerning the compactness of the deposited films. The VOx films generated on stainless steel substrate (Fig. 3c) were composed of two distinct layers: the outer most layer was very compact and dense whereas the inner one was porous and similar to that observed with samples A500 and B500. Such difference could lead to significant differences of electrochemical performances versus Li^+ insertion/extraction into the host lattice. Moreover, even if the deposition of the films were strictly done in the same CVD conditions (pressure, reaction time, etc.), thicker films were observed with Pt substrate (sample A500) indicating a faster kinetic growth using such a substrate. It could therefore explained the cracks onto the surface as shown in Fig. 1a: the too rapid growth kinetic induces larger stress within the film

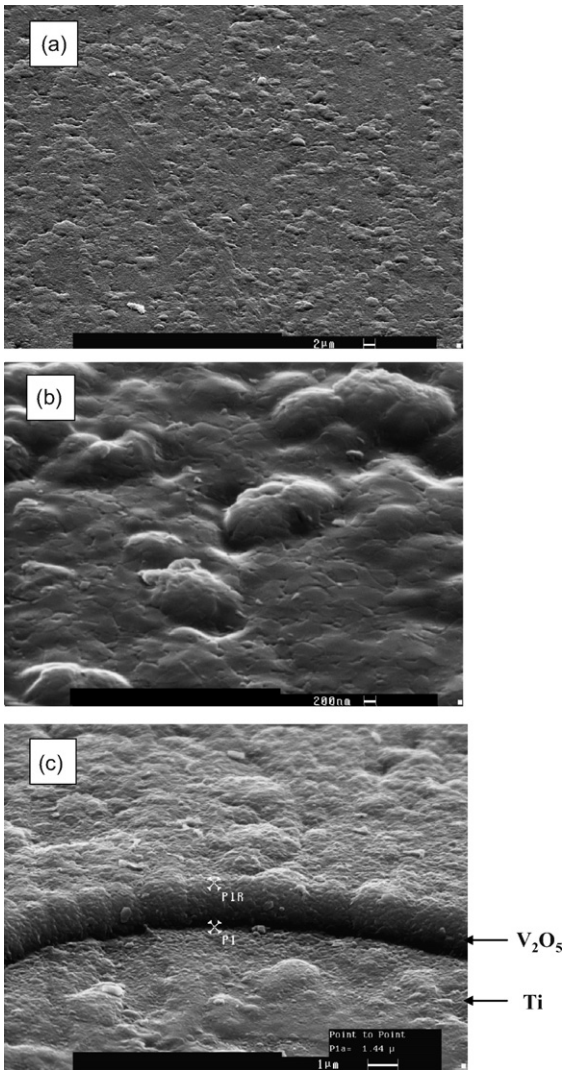

Fig. 2. SEM images of annealed V_2O_5 films deposited by CVD on titanium substrate (sample B500).

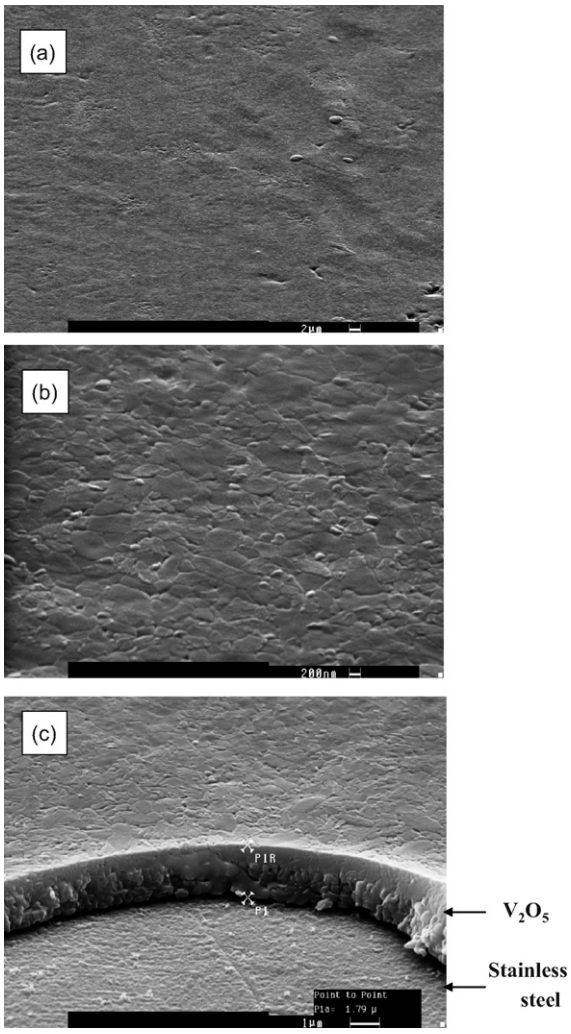

Fig. 3. SEM images of annealed V_2O_5 films deposited by CVD on stainless steel substrate (sample C500).

not only during the thermal annealing but also during the CVD growth.

3.2. XRD measurements on as-deposited VOx films

The influence of the substrate on the composition and the crystallinity of as-deposited vanadium oxides films (i.e. without further thermal annealing) was first studied. Except mica substrate, as-deposited films were green indicating the presence of vanadium with a +IV oxidation state. The XRD patterns of VOx films deposited onto Pt (sample A), Ti (sample B), stainless steel (sample C) and F-doped SnO_2 (sample D) are presented in Fig. 4a–d, respectively. With these substrates, the XRD patterns revealed that the films were non-stoichiometric and composed of a mixture V_2O_5, V_3O_7, V_4O_7 and/or V_5O_9. Only some diffraction lines of these different VOx were observed indicating a poor crystallinity of these vanadium oxides phases. In addition, the low peaks intensities clearly indicated the presence of small amount of the oxides within these films.

In the case of Si substrate (sample G), the as-deposited vanadium oxide films were amorphous since no diffraction lines were pointed out on diffraction patterns (figure not shown here). Similar results were reported by Julien et al. [17] about the amorphous character of VOx films deposited on Si substrate by PLD. With glass (sample E) and mica (sample F) substrates, very different results were observed since the XRD patterns presented in Fig. 4e and f, respectively, have revealed the presence of only V_3O_7 for sample E (Fig. 4e) and V_2O_5 for sample F (Fig. 4f). The XRD pattern obtained with sample F (mica substrate) exhibits the (0 0 2), (0 0 1), (4 0 0) and (0 0 2) diffraction lines at $2\theta = 18^\circ$, 23.6°, 36.3° and 48.2° of polycrystalline orthorhombic V_2O_5. The high intensity of the (0 0 1) peak coupled with the absence of the (1 1 0) diffraction line indicates a much pronounced preferential orientation along *c*-axis. For this sample, the coherence domains (mono-crystal) $D_{0\,0\,1}$ along the *c*-axis were calculated from the broadness of the (0 0 1) peak according to Scherrer's formula given in relation (2). It was found: $D_{0\,0\,1} \approx 34$ nm. Note that the coherence domains $D_{2\,0\,0}$ along the *a*-axis cannot be determined due to the absence of the (2 0 0) diffraction line. For

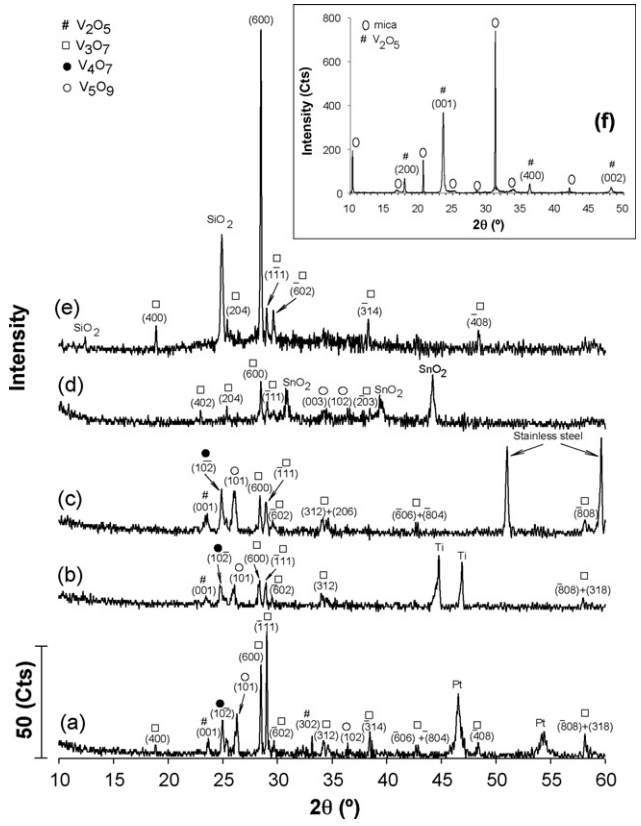

Fig. 4. XRD patterns of as-deposited VOx films deposited by CVD on various substrates: (a) Pt, (b) Ti, (c) stainless steel, (d) F-doped SnO_2, (e) glass and (f) mica.

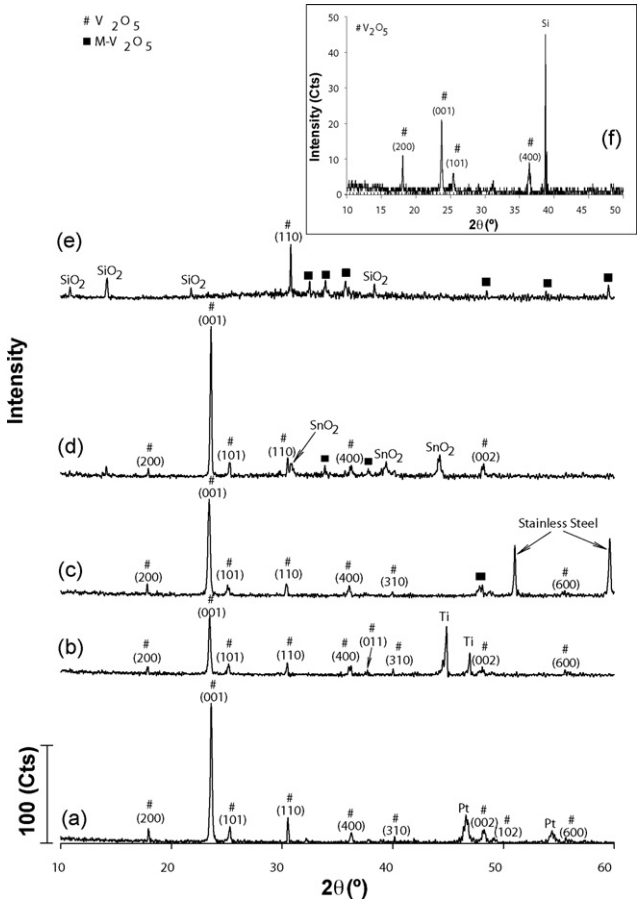

Fig. 5. XRD patterns of annealed VOx films at 500 °C in air deposited by CVD on various substrates: (a) Pt, (b) Ti, (c) stainless steel, (d) F-doped SnO_2, (e) glass and (f) Si.

sample F, the *a* and *c* cell parameters were also deduced from the exploitation of the XRD patterns (orthorhombic V_2O_5 system): $a = 11.47$ Å, and $c = 4.38$ Å. The *b* parameter cannot be determined since the XRD pattern does not exhibit the (1 1 0) diffraction line. These *a* and *c* cell parameter values are very similar to those reported in the literature in the case of well crystallized V_2O_5 obtained by sol–gel method [31], atomic layer deposition [32,33] or RF sputtering [16].

As shown above, the composition of the as-deposited VOx films depends on the substrate. In most of cases, the oxidation state of vanadium of the as-deposited film is lower than +V. To explain the reduction of the vanadium oxidation state, one may consider that a "metallothermic" reduction-type process occurred [34]. Indeed, the feasibility of such a reaction is determined by the free energies of formation of the different compounds involved in the reaction (V_2O_5 and the considered substrate). This reduction process is also influenced by the operating conditions (temperature of the substrate (i.e. of the reaction), concentration of the precursor, pressure in the CVD reactor). Considering the Ellingham–Richardson diagrams given the free energy of formation of the vanadium oxides depending on the nature of the substrate and the reaction temperature, the reduction of vanadium(+V) by Ti, for instance, is possible. In other words, the reduction of V(+V) to lower oxidation state by the substrate has highly favourable free energy values. In contrast, such diagrams show that vanadium(+V) is not reduced by SiO_2 in our experimental conditions, in good agreement with results deduced from XRD measurements. Finally, one can not also exclude the role of carbon in the precursor material which could also be involved in this reduction process of vanadium(+V). Thus, it could explain why, even with Pt substrate which is hardly oxidized, vanadium(+IV) has been detected on XRD patterns (Fig. 4a).

An annealing procedure at 500 °C in air was performed with the same samples to obtain crystalline V_2O_5 and further to study the insertion/extraction of Li^+ when these V_2O_5 films are used as positive electrode in Li-ion batteries.

3.3. XRD measurements on annealed VOx films

Whatever the substrate, the XRD patterns of annealed vanadium oxide films show the diffraction lines of orthorhombic V_2O_5. However, small variation of the film composition was pointed out depending on the substrate (Fig. 5): for sample E500 (glass substrate, Fig. 5e), C500 (stainless steel substrate, Fig. 5c) and D500 (F-doped SnO_2 substrate, Fig. 5d), the other diffraction lines observed on patterns were attributed to the formation of vanadium bronze M–V_2O_5 (M is a cation) formed by reaction with the different substrate.

With Ti, Si and Pt substrates, crystalline V_2O_5 was generated by annealing in air but the amount V_2O_5 crystallites is slightly

different depending on the substrate as attested by the difference in intensities of the diffraction lines. The intensities of the diffraction lines with sample G500 (Si substrate, Fig. 5f) are much lower than those observed with the other one, i.e. V_2O_5 films formed on Si substrate (sample G500) exhibit a lower crystallinity. In addition, one must mention that (i) the intensities of the (h 0 0) diffraction lines are larger than those observed usually with crystalline powder samples, (ii) the low value difference between the intensities of the (2 0 0) and (0 0 1) diffraction lines, (iii) the absence of the (1 1 0) diffraction line. It means that for sample G500, the b-axis is parallel to the substrate.

For sample A500 (Pt substrate, Fig. 5a), sample B500 (Ti substrate, Fig. 5b), sample C500 (stainless steel substrate, Fig. 5c) and sample D500 (F-doped SnO_2 substrate, Fig. 5d), the high intensity of the (0 0 1) diffraction coupled with the high intensities of the (h 0 0) and the presence of the (1 1 0) diffraction line indicates a preferential orientation along the a-axis in the ab plane.

The variations of the coherence domains D_{200} and D_{001} versus the nature of the substrate are reported in Table 1. Rather same D_{200} values were obtained whatever the substrate (around 74 ± 3 nm) except for sample B500 (Ti substrate) for which large values of about 94 nm were obtained. The D_{001}, values do not vary depending on the substrate (around 34 ± 3 nm) except for sample D500 (F-doped SnO_2 substrate) for which a higher value (49.4 nm) was obtained.

The cell parameters deduced from the XRD patterns for V_2O_5 deposited films (orthorhombic V_2O_5 system) after annealing are reported in Table 1. Owing to the presence of the (2 0 0), (1 1 0), and (0 0 1) diffraction lines, it was possible to determine the three a, b and c cell parameters except for sample E500 because of the absence of the (2 0 0) and (0 0 1) diffraction lines on XRD pattern (Fig. 5e). For the other substrates, the cell parameters were roughly the same ($a = 11.52 \pm 3$ Å, $b = 3.56 \pm 1$ Å and $c = 4.39 \pm 1$ Å) and in good agreement with values reported in the literature in the case well crystallized V_2O_5 obtained by other deposition methods [16,31–33].

To summarize, XRD analyses have shown that as-deposited VOx films obtained by CVD using Pt, Ti, stainless steel and F-doped SnO_2, glass substrates were not amorphous and composed of a mixture of V_3O_7, V_4O_7, V_5O_9 and/or V_2O_5. However, pure phases were not obtained directly after deposition except onto mica substrate for which the as-deposited film was composed of crystalline V_2O_5. After annealing, only small structural differences have been pointed out by XRD. The films were mainly composed of orthorhombic V_2O_5 even if in the case of stainless steel, F-doped SnO_2 and glass substrates, a very small amount of vanadium bronze M–V_2O_5 (M is a cation) resulting from the chemical reaction with substrates was pointed out on XRD patterns. The V_2O_5 cell parameters are similar to those reported in the literature in the case of well-crystallized V_2O_5. Finally, rather no variation of the coherence domains along the a-axis and the c-axis was observed depending on the nature of the substrate, except for Ti substrate which exhibited a slightly higher D_{200} value.

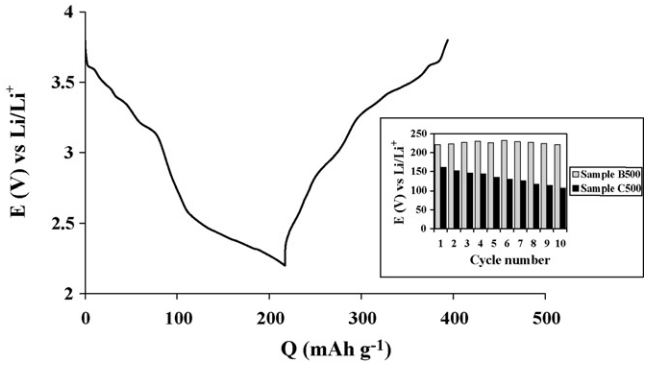

Fig. 6. Tenth charge–discharge chronopotentiogram obtained with sample B500 (Ti substrate) in 1 M $LiClO_4$-PC at room temperature. Potential window for the charge–discharge cycling: 3.8–2.2 V vs. Li/Li^+. Rate: C/23.

Let us consider now the electrochemical performances of samples A500, B500 and C500 when they are used as cathode materials in Li battery.

3.4. Electrochemical properties of annealed VOx films

The initial open circuit voltage of the V_2O_5 film was about 3.43 V versus Li/Li^+ and the charge/discharge curves exhibit the same shape whatever the substrate.

In large potential range (3.8 and 2.2 V versus Li/Li^+), the chronopotentiogram exhibits several plateaus. As an example, the 10th cycle obtained with sample B500 (Ti substrate, thickness of the V_2O_5 film: 1.5 μm) is reported in Fig. 6. The two plateaus observed at around 3.4 and 3.2 V versus Li/Li^+ during charge and discharge procedures are related to phase transitions α–ε and ε–δ which occur in orthorhombic V_2O_5 film concomitant to the Li^+ insertion/extraction. A third plateau at

Table 1
Results deduced from XRD analyses of vanadium oxide films deposited on various substrate

Samples	Substrate	D_{200} (nm)	D_{001} (nm)	a (nm)	b (nm)	c (nm)
A	Pt	71.0	36.7	1.147	0.356	0.438
B	Ti	94.2	35.4	1.153	0.356	0.440
C	Stainless steel	76.6	32.3	1.155	0.357	0.441
D	SnO_2	75.9	49.4	1.149	0.356	0.438
F	Mica	–	34.0	1.147	–	0.438
G	Si	77.0	34.0	1.140	0.350	0.435

D_{200} and D_{001}: coherence domains along the a-axis and the c-axis, respectively, calculated from the broadness of the (2 0 0) and (0 0 1) peaks. Cells parameters values: a, b, c. All films were annealed at 500 °C in air during 2 h except film deposited onto mica substrate for which as-deposited films were composed of crystalline V_2O_5.

around 2.3–2.2 V versus Li/Li^+ due to phase transition δ–γ was observed. By contrast with the shape of chronopotentiograms obtained with composite V_2O_5 electrode, the transition between the plateau at about 3.2 V and the one at 2.3 V is not abrupt and shoulders appear between 2.4 and 2.3 V. The latter may probably result from the occurrence of different phase transitions difficult to determine precisely because of the nature of these phases even by XRD measurements since in that potential window (2.55–2.35 V), the shape of the chronopotentiogram changes during cycling. It could give rise to a shoulder observed during the reverse scan at around 3.5 V versus Li/Li^+. The shoulder pointed out at around 3.6 V versus Li/Li^+ is due to the extraction of Li from γ-LiV_2O_5 [35]. This plateau is small, in comparison with that observed in the case of composite V_2O_5 electrode suggesting that the amount of γ-LiV_2O_5 is low. A high value of about 220 mAh g^{-1} was observed with sample B500 (rate: *C*/23). As shown in the inset of Fig. 6, no capacity fading was observed. In contrast, an important capacity fading has been pointed out with sample C500 (stainless steel substrate, thickness of the V_2O_5 film: 1.8 μm): the capacity observed at the end of the first cycle/discharge cycle was equal to 160 mAh g^{-1} and decreased to about 110 mAh g^{-1} after 10 cycles for a same discharge rate (*C*/23). A reversible capacity value of about 180 mAh g^{-1} was observed for a higher rate (*C*/10) in the case of sample C500. For sample A500 (Pt substrate, thickness of the V_2O_5 film: 3.5 μm), the reversible capacity values in the same potential range (3.8–2.2 V versus Li/Li^+) were lower than those observed with V_2O_5 deposited onto Pt and Ti substrates whatever the current density applied to the electrode: 105 mAh g^{-1} (*C*/30) and 61 mAh g^{-1} (*C*/2).

After cycling in a large potential window, each sample were tested in a smaller potential window (3.8–2.8 V versus Li/Li^+). The 1st and the 20th charge/discharge cycles recorded in this region with sample C500 are presented in Fig. 7a whereas the 1st and the 10th charge/discharge cycles with sample A500 are presented in Fig. 7b. As shown in Fig. 8, the capacity value is roughly constant during cycle life, suggesting no drastic and irreversible changes during charge/discharge cycles whatever the substrate, i.e. no capacity fading was observed in contrast with the results observed (Fig. 6) in a wider potential region (3.8–2.2 V versus Li/Li^+). In this potential range (3.8 and 2.8 V versus Li/Li^+), a different behaviour was observed: the best electrochemical performances were observed with sample C500 for which a capacity of about 115 mAh g^{-1} (rate *C*/23) has been obtained after 20 cycles (Fig. 8). In the case of samples A500 and B500, smaller values close to 82 and 47 mAh g^{-1}, respectively, were obtained after 20 cycles. Such better behaviour in the case of sample C500 was also observed for different current density as shown in Fig. 9.

From these results, it seems to be difficult to establish a clear relationship between the crystal phases and compositions and the electrochemical performances of vanadium oxide films. The XRD measurements did not point out significant differences between the films, except for sample B500 which exhibited the higher coherence domains along the *a*-axis. Nevertheless, one must remind the results deduced from SEM observations. First, as discussed above, the lowest electrochemical performances

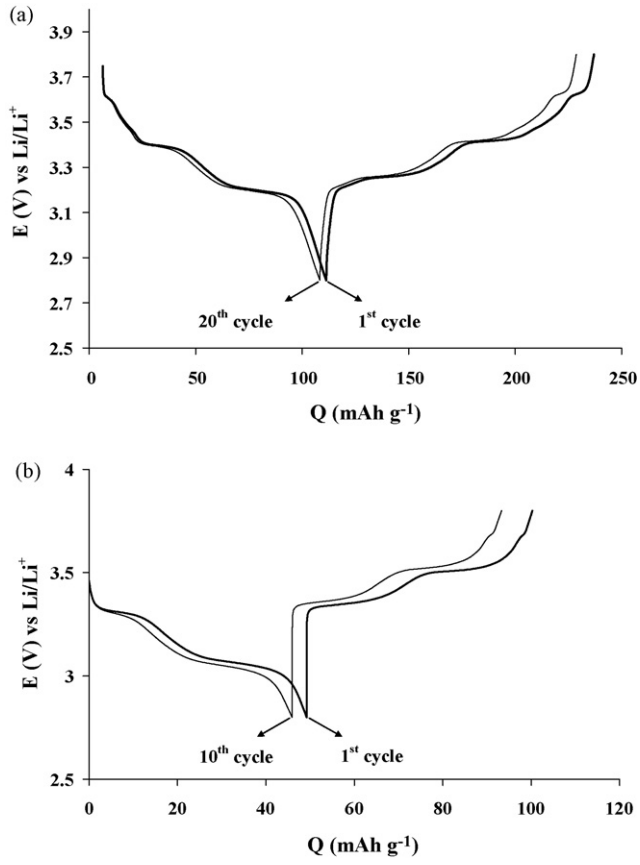

Fig. 7. (a) First and 20th charge–discharge chronopotentiograms obtained with sample C500 and (b) 1st and 10th charge–discharge chronopotentiograms obtained with sample A500 in 1 M $LiClO_4$-PC at room temperature. Potential window for the charge–discharge cycling: 3.8–2.8 V vs. Li/Li^+.

were obtained with sample A500 for which the presence of many cracks on the surface was revealed on SEM images (Fig. 1a). They could induce a loss of adherence of the film onto the surface during the cycle life and could explain the low reversible capacities values. Second, a better homogeneity of the film was observed for sample B500 (Ti substrate) which gave the best electrochemical results in a wide potential range. In contrast, the SEM image of the film deposited onto stainless steel (sample C500) revealed the presence of two distinct layers: the inner layer was similar to that observed with the other substrates, the

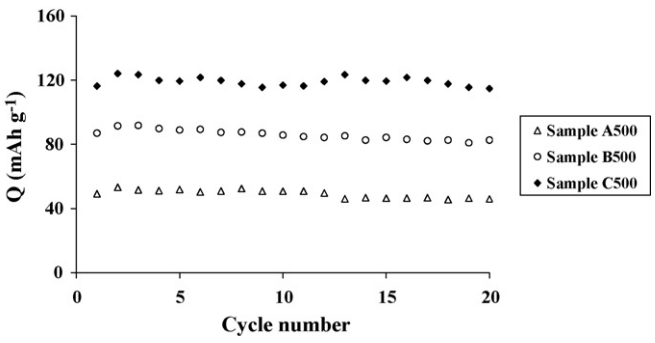

Fig. 8. Evolution of the reversible capacity vs. cycle number depending on the substrate in 1 M $LiClO_4$-PC at room temperature. Potential window for the charge–discharge cycling: 3.8–2.8 V vs. Li/Li^+. Rate: *C*/23.

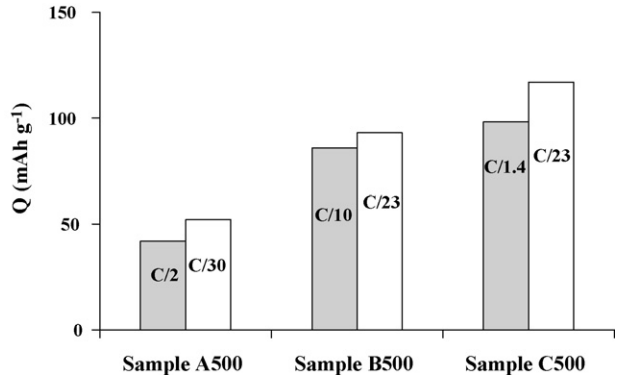

Fig. 9. Evolution of the reversible capacity after 10 cycles depending on the substrate and the current density applied to the electrode in 1 M $LiClO_4$-PC at room temperature. Potential window for the charge–discharge cycling: 3.8–2.8 V vs. Li/Li^+.

outmost layer has a higher compactness. The latter could limit the diffusion pathway for the Li^+ insertion. It could explain why such films did not support the insertion of Li^+ ions in a wide potential region deep.

Consequently, the potential window in which Li^+ ions are inserted/extracted strongly depends on the nature of the substrate. Thus, V_2O_5 film deposited by CVD in our experimental conditions on stainless steel or platinum cannot be cycled in a large potential window whereas it gave rise to the best results in a narrow potential window.

These reversible capacity values can be compared to those obtained with crystalline V_2O_5 films prepared for example by atomic layer chemical vapour deposition (ALCVD) [31]: 125 mAh g^{-1} between 3.8 and 2.8 V versus Li/Li^+ and about 220 mAh g^{-1} between 3.8 and 2.2 V versus Li/Li^+ for V_2O_5 film (thickness of 200 nm) deposited onto a Ti substrate. These values were also in the same order of magnitude as those reported by Navone et al. for thicker V_2O_5 films ($\leq$3.6 μm) prepared by RF sputtering [16] for low charge/discharge rates.

4. Conclusion

Vanadium oxide films were prepared by CVD from pure of triisopropoxyvanadium oxide ($VO(OC_3H_7)_3$) and oxygen as precursors. Depending on the substrate, several types of vanadium oxides were observed. As-deposited films were amorphous except on mica substrate for which crystalline V_2O_5 has been detected from XRD measurements. After annealing at 500 °C in air during 2 h, V_2O_5 was obtained whatever the substrate (Si, glass, F-doped SnO_2, Ti, Pt or stainless steel). The crystallites sizes were not strongly different depending on the substrate: the D_{200} values (along the *a*-axis) were about 74 ± 3 nm except for Ti substrate for with values of about 94 nm were found. Along the *c*-axis, the D_{001} were roughly constant and close to 35 ± 2 nm, except for F-doped SnO_2 substrate for which values of about 49 nm were observed.

Whatever the substrate, SEM images revealed the presence of typical V_2O_5 plates [32] but the kinetic growth seems to be dependent on the nature of the substrate since different film thicknesses were observed in spite of the fact that same CVD operating conditions have been used for their synthesis.

When the annealed V_2O_5 films were used as cathode materials in secondary lithium batteries, small structural changes were observed during cycling even at low potential. The best electrochemical performances were also observed with V_2O_5 deposited onto stainless steel substrate between 3.8 and 2.8 V versus Li/Li^+ whereas the best ones were observed with films deposited onto Ti substrate between 3.8 and 2.2 V versus Li/Li^+.

Acknowledgments

The authors are grateful to the LCAES-CNRS UMR 7574 (ENSCP, Paris) for their assistance in experimental work for XRD determinations, Dr. S. Borensztajn for SEM determinations, and M.P. Genevois for his helpful assistance in making the electrochemical cells used in this study. We are grateful to JIPELEC for having lent the INJECT liquid delivery and vaporization system and for technical support and assistance.

References

[1] C. Julien, in: S. Radhakrishna (Ed.), Trends in Materials Science, Narosa Publishing House, London, 1996, p. 24.
[2] B. Scrosati, in: C.A. Vincent, B. Scrosati (Eds.), Modern Batteries, 2nd ed., Arnold, London, 1997, p. 199 (Chapter 7).
[3] M. Wakihara, Mater. Sci. Eng. R 33 (2001) 109.
[4] G. Pistoia, Batteries for Portable Devices, Elsevier, Amsterdam, 2005.
[5] J.-P. Pereira-Ramos, N. Baffier, G. Pistoia, in: G. Pistoia (Ed.), Lithium Batteries: New Materials, Developments and Perspectives, Elsevier, Amsterdam, 1994, p. 281.
[6] M.S. Whittingham, Prog. Solid State Chem. 12 (1978) 41.
[7] E. Potiron, A. Le Gal La Salle, A. Verbaere, Y. Piffard, D. Guyomard, Electrochim. Acta 45 (1999) 197.
[8] N. Kumagai, H. Kitanoto, M. Baba, S. Durand-Vidal, H. Groult, D. Devilliers, J. Appl. Electrochem. 28 (1998) 41.
[9] K. Le Van, H. Groult, A. Mantoux, L. Perrigaud, F. Lantelme, R. Lindström, R. Baddour-Hadjean, S. Zanna, D. Lincot, J. Power Sources 160 (2006) 592.
[10] V. Vivier, J. Farcy, J.-P. Pereira Ramos, Electrochim. Acta 44 (1998) 831.
[11] C. Julien, I. Ivanov, A. Gorenstein, Mater. Sci. Eng. B 33 (1995) 168.
[12] J.-G. Zhang, J.M. McGraw, J. Turner, D. Ginley, J. Electrochem. Soc. 144 (1997) 1630.
[13] D.W. Murphy, P.A. Christian, Science 205 (1979) 651.
[14] J.B. Bates, G.R. Gruzalski, N.J. Dudney, C.F. Luck, X.H. Yu, S.D. Jones, Solid State Tech. 36 (7) (1993) 59.
[15] A. Mantoux, H. Groult, E. Balnois, P. Doppelt, L. Gueroudji, J. Electrochem. Soc. 151 (2004) A368.
[16] C. Navone, J.-P. Pereira-Ramos, R. Baddour-Hadjean, R. Salot, J. Electrochem. Soc. 153 (2006) A2287.
[17] C. Julien, E. Haro-Poniatowski, M.A. Camacho-Lopez, L. Escobar-Alarcon, J. Jimenez-Jarquin, Mater. Sci. Eng. B 65 (1999) 170.
[18] M.Y. Saïdi, R. Koksbang, E.S. Saïdi, H. Shi, J. Barker, J. Power Sources 68 (1997) 726.
[19] D.W. Murphy, P.A. Christian, F.J. DiSalvo, J.N. Carides, J.V. Waszczak, J. Electrochem. Soc. 128 (1981) 2053.
[20] K.M. Abraham, J.L. Goldman, M.D. Dempsey, J. Electrochem. Soc. 128 (1981) 2493.
[21] R. Lindström, V. Maurice, H. Groult, L. Perrigaud, S. Zanna, C. Cohen, P. Marcus, Electrochim. Acta 51 (2006) 5001.
[22] A. Gies, B. Pecquenard, A. Benayad, H. Martinez, D. Gonbeau, H. Fuess, A. Levasseur, Solid State Ionics 176 (2005) 1627.
[23] M. Menetrier, A. Levasseur, C. Delmas, Mater. Sci. Eng. B 3 (1989) 103.
[24] C. Léger, S. Bach, P. Soudan, J.-P. Pereira-Ramos, J. Electrochem. Soc. 152 (2005) A236.

[25] F. Cardarelli, in: J.-E. Mittelman (Ed.), Materials Handbook, Springer, London, 2000, p. 118.
[26] N. Sonoyama, T. Hiraide, T. Abe, M. Minoura, A. Yamada, K. Tamura, J. Mizuki, R. Kanno, Proceedings of the IMLB 2006, Biarritz, France, 2006 (Abstract 354).
[27] S.T. Oyama, G.A. Somorjai, J. Phys. Chem. 94 (1990) 5022.
[28] H. Meixner, J. Gerblinger, U. Lampe, M. Fleischer, Sens. Actuators B 23 (1995) 119.
[29] P. Doppelt, Coord. Chem. Rev. 178–180 (1998) 1785.
[30] B.E. Warren, Phys. Rev. 59 (1941) 693.
[31] P. Soudan, J.-P. Peirera-Ramos, J. Farcy, G. Grégoire, N. Baffier, Solid State Ionics 135 (2000) 291.
[32] H. Groult, E. Balnois, A. Mantoux, K. Le Van, D. Lincot, Appl. Surf. Sci. 252 (2006) 5917.
[33] A. Mantoux, Thesis, P. & M. Curie University, Paris, 2003.
[34] R. Ressel, M. Hochenhofer, H. Antrekowitsch, in: M.E. Schlesinger (Ed.), Proceedings of the EPD Congress 2005, The Materials, Metals & Materials Society (TMX), 2005, p. 763.
[35] C. Delmas, H. Cognac-Auradou, J.M. Cocciantelli, M. Ménetrier, J.P. Doumerc, Solid State Ionics 69 (1994) 257.